

Threshold size for the emergence of classical-like behavior

Alessandro Coppo^{1,2}, Nicola Pranzini^{3,4} and Paola Verrucchi^{5,1,2}

¹*Dipartimento di Fisica e Astronomia, Università di Firenze, Sesto Fiorentino, 50019 Florence, Italy*

²*INFN, Sezione di Firenze, Sesto Fiorentino, 50019 Florence, Italy*

³*QTF Centre of Excellence, Department of Physics, University of Helsinki, PO Box 43, 00014 Helsinki, Finland*

⁴*InstituteQ: The Finnish Quantum Institute, University of Helsinki, 00014 Helsinki, Finland*

⁵*UOS Dipartimento di Fisica, ISC-CNR, Università di Firenze, Sesto Fiorentino, 50019 Florence, Italy*



(Received 9 May 2022; accepted 1 September 2022; published 13 October 2022)

In this work we design a procedure to estimate the minimum size beyond which a system is amenable to a classical-like description, i.e., a description based on representative points in classical phase spaces. This is obtained by relating quantum states to representative points via generalized coherent states (GCSs) and designing a positive-operator-valued measure (POVM) for GCS discrimination. Conditions upon this discrimination are defined such that the POVM results convey enough information to meet our needs for reliability and precision, as gauged by two parameters ϵ , of our arbitrary choice, and δ , set by the experimental apparatus, respectively. The procedure implies a definition of what is meant by the “size” of the system, in terms of the number N of elementary constituents that provide the global algebra leading to the phase space for the emergent classical-like description. The above conditions on GCS discrimination can be thus turned into $N > N_t(\epsilon, \delta)$, where $N_t(\epsilon, \delta)$ is the threshold size mentioned in the title. The specific case of a magnetic system is considered, with details of a gedanken experiment presented and thoroughly discussed. Results for pseudospin and bosonic systems are also given.

DOI: [10.1103/PhysRevA.106.042208](https://doi.org/10.1103/PhysRevA.106.042208)

I. INTRODUCTION

The profound difference between classical and quantum physics fosters the idea that systems are either classical or quantum, as if the adjectives refer to an intrinsic nature of physical objects. The idea is wrong: It is just a matter of what scientific theory best describes the behavior of the system under analysis, in the regime of parameters in which one is interested. Moreover, the recent advancements in quantum technologies urge the adoption of a viewpoint from which classical and quantum features can be seen together and the origin of the former from the latter is clear. In fact, a functioning quantum device acts as a mediator between elementary quantum components (such as the qubits) and complex classical-like apparatuses (including human beings), in a way such that a quantum treatment of the latter is out of reach and a classical-like description of the former might be inadequate. The same quest for a hybrid quantum-classical approach arises in the framework of cosmology, where macroscopic objects manifest themselves according to the laws of classical physics, via general relativity, and yet have quantum traits, as is the case of black holes and their Hawking radiation [1]. In this respect, one should bear in mind that macroscopicity in itself does not guarantee the obliteration of quantum features, unless further assumptions are made [2–5].

In this work we show that results from quantum measurements can produce acceptable (in terms of reliability and precision) classical-like descriptions of large enough systems, with the size represented by the number N that counts their elementary constituents, degrees of freedom, dynamical

variables, or whatever such that $N \rightarrow \infty$ is a necessary condition for a classical-like behavior to emerge. Our result consists in defining a fit as a positive-operator-valued measure (POVM) [6–8] and derive a threshold value of N above which its outcomes allow one to identify the classical state of the system, i.e., its representative point on a classical phase space, precisely enough to provide the required accuracy, given the resolution of the available measuring apparatus. A paradigmatic spin system is explicitly considered to serve as an example and give a figure for the threshold value.

The structure of the paper is as follows. In Sec. II we introduce generalized coherent states (GCSs) and their relevant properties with respect to the large- N limit, defined in Sec. III. The POVM for GCS discrimination is defined in Sec. IV, where we set the conditions ensuring that a classical-like description can emerge from the POVM results themselves. In Sec. V we consider the case of a magnetic system, for which we describe a gedanken experiment realizing the above-mentioned POVM and discuss the possible use one can make of its results as N is varied. Results for pseudospin and bosonic systems are provided in Sec. VI, where we discuss some general consequences of these results. Details of some formal aspects are given in Appendixes A–C, while in Appendix D a superposition of GCSs is considered.

II. COEXISTENCE OF QUANTUM AND CLASSICAL: GENERALIZED COHERENT STATES

A powerful tool for studying problems where quantum and classical features coexist is the formalism of GCSs, which

provides a common semantic framework for quantum and classical physics. Their group-theoretic construction goes as follows [9–11].

Consider a quantum theory defined¹ by a Lie algebra \mathfrak{g} and a unitary irreducible representation of the corresponding group G on some Hilbert space \mathcal{H} . Notice that, by definition, this group contains all the possible time-evolution operators of the system, whence the epithet “dynamical group.” Choose a state (normalized vector) $|R\rangle \in \mathcal{H}$ and identify the elements of G that leave $|R\rangle$ unchanged up to an irrelevant phase factor: It is easily checked that they form a normal subgroup $F \subset G$ and hence define a quotient G/F . Generalized coherent states are defined as

$$|\Omega\rangle := \hat{\Omega} |R\rangle, \quad \hat{\Omega} \in G/F. \quad (1)$$

Each $\hat{\Omega} \in G/F$ is related, by definition, to a GCS $|\Omega\rangle$; moreover, the quotient-manifold theorem [12] ensures that each $\hat{\Omega}$ is biunivocally associated with a point Ω of a manifold \mathcal{M} , which is demonstrated to be symplectic [9], with the properties of a phase space. This establishes one of the main traits of GCSs, namely, that each coherent state $|\Omega\rangle \in \mathcal{H}$ is univocally related to the representative point of a physical state, $\Omega \in \mathcal{M}$, as intended by the classical Hamiltonian formalism. Another relevant feature of GCSs is that a system in a GCS will always evolve into another GCS (a statement that is often summarized in the motto “once a coherent state, always a coherent state” [9]), due to the fact that GCSs form a closed set with respect to the action of any element of G , according to their definition (1), and G contains all the time-evolution operators of the system, as noted above. Therefore, assuming that Γ is in a GCS at a certain time guarantees it will be in a GCS at any later time, which is why one can say that the quantum unitary dynamics of GCSs defines trajectories on \mathcal{M} .

Generalized coherent states are normalized but nonorthogonal and provide a resolution of the identity on \mathcal{H} via $\int_{\mathcal{M}} d\mu(\Omega) |\Omega\rangle \langle \Omega| = \hat{\mathbb{1}}$, where $d\mu(\Omega)$ is invariant with respect to the action of the operators $\hat{\Omega}$. When \mathfrak{g} admits a Cartan decomposition into diagonal operators $\{\hat{H}_i\}_{\mathcal{I}}$ and shifts $\{\hat{E}_\alpha\}_{\mathcal{A}}$, one can write $\hat{\Omega} \in G/F$ as $\hat{\Omega} = \exp \sum_{\alpha \in \mathcal{A}} (\Omega_\alpha \hat{E}_\alpha - \Omega_\alpha^* \hat{E}_\alpha^\dagger)$ and hence, from Eq. (1),

$$|\Omega\rangle = \exp \left(\sum_{\alpha \in \mathcal{A}} \Omega_\alpha \hat{E}_\alpha - \Omega_\alpha^* \hat{E}_\alpha^\dagger \right) |R\rangle, \quad (2)$$

where Ω_α are complex numbers that provide the coordinates of the point $\Omega \in \mathcal{M}$. From Eq. (2) one obtains coherent states for $\mathfrak{su}(2)$ (spin CSs) and for $\mathfrak{su}(1, 1)$ (pseudospin CSs). Despite not admitting a Cartan decomposition, a lookalike expression defines coherent states also for the two algebras \mathfrak{h}_4 and \mathfrak{h}_6 (the well-known bosonic CSs and their squeezed version, respectively).

We will hereafter write \mathfrak{g} CSs to indicate coherent states relative to the specific algebra \mathfrak{g} . Expectation values of one-

dimensional projectors upon GCSs

$$\langle \Omega | \phi \rangle \langle \phi | \Omega \rangle = |\langle \Omega | \phi \rangle|^2 := H_{|\phi\rangle}(\Omega) \quad (3)$$

are often called Husimi functions and are normalized probability distributions on \mathcal{M} for whatever normalized element $|\phi\rangle \in \mathcal{H}$, there included another GCS [13,14]. Among the consequences of this fact, most relevant to this work is that it allows one to define a distance between quantum states in terms of the distance between probability distributions named after Monge [15,16]. In fact, it was demonstrated [17] that the Monge distance between $H_{|\phi\rangle}(\Omega)$ and $H_{|\psi\rangle}(\Omega)$ is a legitimate distance between $|\phi\rangle$ and $|\psi\rangle$, which we will hereafter indicate as $d_M(|\phi\rangle, |\psi\rangle)$ and simply dub Monge distance. Evaluating $d_M(|\phi\rangle, |\psi\rangle)$ requires dealing with a transportation problem [18] which is most often too complex to solve. However, the Monge distance bears properties that make its use very convenient when GCSs are involved and the quantum-to-classical crossover is considered, as further commented upon in the next section and in Appendix A.

III. WHEN QUANTUM BEHAVES CLASSICALLY: THE LARGE- N LIMIT

A formal description of how and under what conditions a physical system displays a behavior that can be described by the laws of classical physics is provided by the so-called large- N limit approach, developed in the framework of quantum field theory several decades ago [2,19,20]. A cornerstone of this approach is the fact that a macroscopic system, whose size is gauged by the number N mentioned in the Introduction, may or may not display a classical-like behavior: The former is true if some conditions hold, which are given in terms of GCSs and provide the details of the effective classical theory obtained in the $N \rightarrow \infty$ limit [3,21]. A definition of N is not generally available and its identification is not always evident. In fact, the best way to recognize N in the specific problem under analysis is to look for a parameter that can grow infinitely, in realizing the above-mentioned conditions. In particular, for $N \rightarrow \infty$ the Lie brackets (or their representation as commutators) must vanish so as to push the lower bound of any uncertainty relation of the theory down to zero, and the invariant measure entering the resolution of the identity on \mathcal{H} must be

$$d\mu(\Omega) = c_N dm(\Omega), \quad (4)$$

with $dm(\Omega)$ a measure on \mathcal{M} properly scaled, via the N -dependent positive constant c_N , so as to make $\int_{\mathcal{M}} dm(\Omega)$ independent of N itself. Moreover, it must be

$$\lim_{N \rightarrow \infty} N |\langle \Omega | \Omega' \rangle|^2 = \delta(\Omega - \Omega') \quad (5)$$

for any pair of GCSs $|\Omega\rangle$ and $|\Omega'\rangle$, meaning that a notion of distinguishability between GCSs is recovered along the quantum-to-classical crossover. In fact, it has been demonstrated [17,22] that when Eq. (5) holds, the Monge distance $d_M(|\Omega\rangle, |\Omega'\rangle)$ between GCSs flows into the metric-induced distance $d(\Omega, \Omega')$ between points on \mathcal{M} . This reinforces the affinity between the algebraic quantum description with GCSs and the geometrical classical one with representative points, establishing that if the distance between two representative

¹The Lie algebra that defines a quantum theory is the one whose irreducible representation on the Hilbert space of the system that the theory describes contains the Hamiltonian and all the relevant observables of the system itself.

points is large enough to be appreciated, then the GCSs associated with those two points must become distinguishable in the large- N limit. It can also be demonstrated (see Ref. [22] and Appendix A for more details) that

$$d_M(|\Omega\rangle, |\Omega'\rangle) \leq d(\Omega, \Omega'), \quad (6)$$

implying that the Monge distance cannot provide a precision in GCS discrimination higher than that granted by the metric-induced distance for classical states recognition. Finally, as Eq. (5) holds in the $N \rightarrow \infty$ limit, there should exist a large- N twilight zone where a classical-like analysis of the system behavior is possible (large N) and yet some of its quantum features are retained (finite N). This is the situation in which we are interested the most, which we propose to characterize as follows.

IV. CLASSICAL-LIKE DESCRIPTION VIA QUANTUM MEASUREMENTS

Consider a system Γ with Hilbert space \mathcal{H} and GCS $\{|\Omega\rangle\}_{\mathcal{H}}$, with \mathcal{M} the related symplectic manifold. We ask whether the behavior of Γ is amenable to an effective classical-like description. In other words, can we experimentally determine the coordinates of a point in some phase space that embody enough information on Γ to be considered representative of its state, in a classical sense? To get a positive answer, we first require that Γ be in a GCS; this choice is based on the fact that such states are demonstrated to survive the above large- N limit as proper physical states [2,3,19,20]. However, they might not be the only ones; in fact, whether or not a GCS is a necessary condition for a quantum state to flow into a well-defined classical one is not known yet (see Sec. VII of Ref. [2] for a thorough discussion of this point). Tackling this issue goes beyond the purpose of this work; however, for the sake of thoroughness, in Appendix D we consider the case when Γ is in a superposition of two GCSs. Returning to our procedure, once we assume that Γ is in a GCS, we will check if an effective discrimination procedure [23] for GCSs can be designed. Notice that since we assume the system to be in a GCS and given that it can only evolve into another GCS, a discrimination procedure that works for whatever GCS will faithfully describe also the system evolution, as further commented upon in Sec. VI.

In fact, if we can tell that Γ is in a specific GCS $|\Sigma\rangle$, a classical-like description emerges from the one-to-one relation between the element $|\Sigma\rangle \in \mathcal{H}$ and the point Σ in the symplectic manifold \mathcal{M} , now intended as a classical phase space. Therefore, our program goes as follows: (i) Design a POVM for GCS discrimination, (ii) analyze the conditions under which the corresponding measurement meets our demand for sharpness, and (iii) find a value N_t such that $N > N_t$ ensures the above conditions are fulfilled.

(i) *POVM for GCS discrimination.* We introduce a tessellation of \mathcal{M} by choosing a separable set of regions

$$\begin{aligned} I_i \in \mathcal{M}, i = 1, \dots, L \\ \text{s.t. } \cup_j I_j = \mathcal{M}, I_i \cap I_{j \neq i} = \emptyset; \end{aligned}$$

we call these regions tiles. We establish that each tile I_i is biunivocally associated with one possible result m_i of our

gedanken experiment and define the effects

$$\hat{E}_i = \hat{E}(m_i) := \int_{I_i} d\mu(\Omega) |\Omega\rangle \langle \Omega|, \quad (7)$$

with $|\Omega\rangle$ the GCS of the system. As the index $i = 1, \dots, L$ counts the distinguishable results that the instrument provides, a larger L implies a higher resolution of our instrument. It is easily checked that the above effects are positive-semidefinite operators that sum up to the identity on \mathcal{H} such that

$$\hat{E}(\cup_j m_j) = \int_{\cup_j I_j} d\mu(\Omega) |\Omega\rangle \langle \Omega| = \sum_j \hat{E}_j; \quad (8)$$

therefore, they define a POVM, with the probability to get the result m_i , when Γ is in a state $|\phi\rangle$, given by the Born rule $p_{|\phi\rangle}(m_i) = \text{Tr}[\hat{E}_i |\phi\rangle \langle \phi|]$. When $|\phi\rangle$ is a GCS, say, $|\Sigma\rangle$, the invariance of $d\mu(\Omega)$ and the definition of the GCS via Eq. (1) imply

$$p_{|\Sigma\rangle}(m_i) = \text{Tr}[\hat{E}_i |\Sigma\rangle \langle \Sigma|] = \int_{I_i} d\mu(\Omega) |\langle \Sigma | \Omega \rangle|^2. \quad (9)$$

If the representation of \mathfrak{g} is infinite dimensional, the effectively accessed states of the system are assumed to belong to a finite-dimensional subspace $\tilde{\mathcal{H}} \subset \mathcal{H}$ and the apparatus will be asked to explore just a compact portion $\tilde{\mathcal{M}}$ of \mathcal{M} . A properly normalized measure $d\tilde{\mu}(\Omega)$ will ensure that $\int_{\tilde{\mathcal{M}}} d\tilde{\mu}(\Omega) |\Omega\rangle \langle \Omega| = \mathbb{1}_{\tilde{\mathcal{H}}}$. For the sake of simplicity, we will hereafter assume that \mathcal{M} is compact.

As GCSs are not orthogonal, from Eq. (9) it follows that $p_{|\Sigma\rangle}(m_i) > 0$ for all m_i and whatever the GCS $|\Sigma\rangle$: Therefore, the above POVM cannot provide a proper GCS discrimination. However, we can settle for an approximate discrimination of this type: We choose one point Λ_i in each tile I_i , thus establishing the chain of biunivocal relations

$$m_i \leftrightarrow \Lambda_i \leftrightarrow |\Lambda_i\rangle \quad (10)$$

and require $p_{|\Lambda_i\rangle}(m_i) = \delta_{ij}$ to guarantee perfect discrimination at least between GCSs of the set $\{|\Lambda_i\rangle\}$, hereafter called sampled GCSs. As for other GCSs, we introduce the patch \tilde{I}_i , made of I_i and its neighboring tiles (see Fig. 1), and demand that a result m_i informs us that Γ is in a GCS whose representative point surely belongs to \tilde{I}_i . In order to obtain the above type of GCS discrimination, we first consider null any inner product whose modulus is less than a chosen (small) positive value ϵ [we will hereafter use the symbol \sim for (in)equalities that only hold subject to this choice]; a notion of ϵ orthogonality follows, defined by $|\langle \Sigma | \Omega \rangle| \leq \epsilon \Leftrightarrow |\Sigma\rangle, |\Omega\rangle$ are ϵ orthogonal, which carries the possibility to consider two GCSs distinguishable if their respective Husimi functions are never simultaneously larger than ϵ^2 . This can be illustrated, for instance, by plotting the sum of two Husimi functions $H_{|\Sigma\rangle}(\Omega) + H_{|\Sigma'\rangle}(\Omega)$ and the plane marking the value $2\epsilon^2$, as done in Fig. 2 for different values of N : If the sum emerges from the plane in the form of two distinct peaks, the respective GCSs $|\Sigma\rangle$ and $|\Sigma'\rangle$ are distinguishable in the sense of the ϵ orthogonality introduced above. After this choice, for each GCS $|\Sigma\rangle$ we define the region

$$S_{|\Sigma\rangle}^\epsilon = \{\Omega \in \mathcal{M} : |\langle \Sigma | \Omega \rangle| > \epsilon\} \quad (11)$$

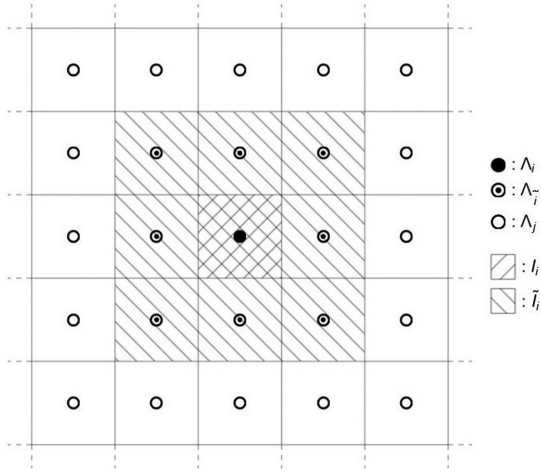


FIG. 1. Example of tessellation of a portion of plane, with tiles (squares) and sampled points (open circles). The patch \tilde{I}_i and its reference tile I_i are shown, together with their respective sampled points $\Lambda_{\tilde{i}}$ and Λ_i , as indicated alongside the image.

that contains all the representative points of GCSs that are not ϵ orthogonal with $|\Sigma\rangle$. Note that, due to condition (5), the region $S_{|\Sigma\rangle}^\epsilon$ shrinks as $N \rightarrow \infty$, which allows one to choose an ever smaller value of ϵ in such limit.

(ii) *Conditions for a sharp enough GCS discrimination.* We consider a GCS discrimination sharp enough to provide an acceptable classical-like description of Γ via the results of the POVM (7) if conditions

$$S_{|\Lambda_i\rangle}^\epsilon \subseteq I_i \forall i, \quad (12)$$

$$S_{|\Sigma\rangle}^\epsilon \subseteq \tilde{I}_i \forall \Sigma \in I_i \quad (13)$$

hold. While the first condition makes sampled GCSs distinguishable, the second one means $|\langle \Sigma | \Omega \rangle| \simeq 0$ for $\Omega \notin \tilde{I}_i$, i.e., $p_{|\Sigma\rangle}(m_i) \sim 0$ if $\Sigma \notin \tilde{I}_i$, thus giving the output m_i the information content mentioned above.

Note that any tessellation implementing a POVM defined by Eqs. (7)–(9) and such that the conditions (12) and (13) are satisfied guarantees a GCS discrimination that can be interpreted as a classical limit (as this possibility follows from \mathcal{M} being symplectic, with the properties of a classical phase space, and GCSs staying in one-to-one relation with its points). However, this does not necessarily imply that the emerging description is faithful. In particular, if the tiles are quite nonuniform in size and/or the shape of some tiles I_j is essentially different from that of the corresponding $S_{|\Lambda_j\rangle}^\epsilon$, the above phase space will be irregularly sampled and the classical description might become distorted, a situation that corresponds, in our approach, to a badly designed experimental apparatus. On the most general level, when neither the manifold \mathcal{M} nor the GCS are specified, the distortion due to the nonuniform size can be kept under control by using a unique parameter to gauge the extension of all the tiles, which is what we propose in the following point (iii). Additionally, when a specific case is considered, meaning that \mathcal{M} and the shape of the regions $S_{|\Lambda_j\rangle}^\epsilon$ are known, the tessellation can be designed explicitly to avoid the above-mentioned shape

mismatch, as done in the example of Sec. V and thoroughly discussed in Appendix B.

(iii) *Value of N ensuring that the conditions (12) and (13) are fulfilled.* Finding this value generally requires the analysis of geometrical properties that depend on \mathcal{M} and can be very difficult to deal with. Therefore, we choose to replace the conditions (12) and (13) with an algebraic inequality, faithful to their meaning but easier to study. To this aim, we remove the arbitrariness in the definition of the tiles I_i by introducing a parameter δ defined, for instance, as

$$\delta := \min_j \left\{ \min_{\Omega \in \partial I_j} d(\Omega, \Lambda_j) \right\}, \quad (14)$$

where ∂I_j is the border of the j th tile. In words, δ is the minimum value taken by the radius of the largest circle centered in Λ_j and fully contained in I_j , given the tessellation. In fact, δ is most generally defined by Eq. (B3); however, for the sake of clarity, we use here the simpler definition (14). As δ gauges the extension of the tiles, a smaller δ implies a larger L and hence a better resolution of our instrument. This gives the tiles a further dependence on δ , which is why we will hereafter indicate them as I_i^δ . Then we replace (12) and (13) with

if $\Sigma \in I_i^\delta$ then

$$|\langle \Sigma | \Omega \rangle| > \epsilon \Rightarrow d_M(|\Omega\rangle, |\Lambda_i\rangle) \leq \delta + d_M(|\Sigma\rangle, |\Lambda_i\rangle). \quad (15)$$

The distinguishability between sampled GCSs required by (12) is granted by (15) with $\Sigma = \Lambda_i$. On the other hand, whether or not an exact match between (13) and (15) exists depends on the geometry of the problem, the tessellation chosen, and the definition of the parameter δ . In particular, the latter can be taken to be different from Eq. (14) to translate (12) and (13) into (15) in a way that better corresponds to the specific problem and experimental apparatus one is considering (see Appendix B for more comments on this). We also underline that using the distance between points induced by the metric on \mathcal{M} , instead of the Monge distance between quantum states in \mathcal{H} , would be incorrect, as the geometrical distance between points on a manifold is generally unrelated to whatever the distance is between quantum states, even if only GCSs are considered. However, the Monge distance has the advantage of carrying the ordering relation (6), so that enforcing (15) with d rather than d_M ensures that (15) itself is fulfilled. Consistently, using one or the other distance becomes equivalent as $N \rightarrow \infty$. This is seen, for instance, in Fig. 9 of Appendix A, where d_M between two $\text{su}(2)$ GCSs as a function of N [22] is compared with the value of the (constant) metric-induced distance between their respective representative points, as a function of N .

Finally, as the region $S_{|\Sigma\rangle}^\epsilon$ shrinks when N increases, according to Eq. (5) and as seen in Fig. 2, we expect that a finite threshold value $N_t(\epsilon, \delta)$ exists such that

$$N > N_t(\epsilon, \delta), \quad (16)$$

which implies that the condition (15) is fulfilled. The dependence of N_t on ϵ and δ reminds us that a critical size does not exist beyond which a system behaves according to the laws of classical physics. Rather, it all depends on the goggles we wear, here designed by ϵ and δ . However, if $N > N_t$ the result of one single experiment, say, m_i , conveys a meaningful piece of information, namely, that Γ is surely described by a GCS

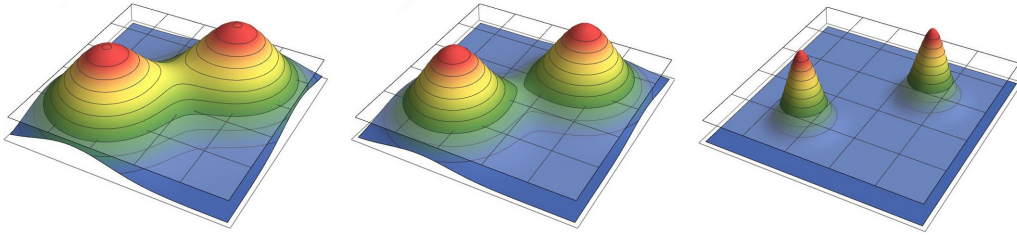


FIG. 2. Plot of ϵ orthogonality in the bosonic case: The sum of two Husimi functions, for two different bosonic GCSs on the complex plane. The translucent plane indicates the value of $2\epsilon^2$. The number N grows from left to right. Correspondingly, the two GCSs are not ϵ orthogonal in the left panel and increasingly ϵ orthogonal in the middle and right ones.

in \tilde{I}_i and, with a fair degree of certainty (gauged by ϵ and δ), by the sampled GCS $|\Lambda_i\rangle$ itself. In the language of classical physics, the same holds, with GCSs replaced by representative points in the system's phase space. For the sake of clarity, in the next section we consider a specific case and show how to locate $N_t(\epsilon, \delta)$ explicitly.

V. GEDANKEN EXPERIMENT

In this section we consider a composite magnetic system Γ with total spin (or angular) momentum fixed to J , due to some constraint upon the accessible quantum states of its N subsystems. The system can be made, for instance, by a number N of spin- $\frac{1}{2}$ particles, each localized on a site of a ring (see Fig. 3) and interacting with its two nearest neighbors via an isotropic Heisenberg interaction or anything else leading to a total Hamiltonian that commutes with the total spin operator. The quantum theory that describes this system is defined by the Lie algebra $\mathfrak{su}(2)$, which is a vector space spanned by the set $\{J_0, J_1, J_2\}$, with Lie brackets $[J_i, J_j] = i\epsilon_{ijk}J_k$ and Casimir $\mathbf{J}^2 = J_0^2 + J_1^2 + J_2^2$. Each irreducible representation of the algebra is labeled by an integer or half-integer number $J = \frac{1}{2}(N - n)$, for some positive integer $n \leq N$, associated with the Casimir operator via $\hat{\mathbf{J}}^2 = J(J + 1)\hat{\mathbb{1}}_{\mathcal{H}_J}$, where \mathcal{H}_J is

the Hilbert space carrying the representation, with $\dim \mathcal{H}_J = 2J + 1$. The spectrum of \hat{J}_0 is $m = -J, -J + 1, \dots, J - 1, J$ and its eigenvectors $\hat{J}_0 |J, m\rangle = m |J, m\rangle$ span \mathcal{H}_J .

The manifold \mathcal{M} introduced in Sec. II is the sphere S_2 , and choosing $|R\rangle = |J, m = -J\rangle$ in Eq. (2), an $\mathfrak{su}(2)$ CS reads

$$|\Omega\rangle = \sum_{m=-J}^J g_m(\Omega) |J, m\rangle, \quad (17)$$

where $\Omega = \frac{\theta}{2}e^{-i\phi}$ identifies a point on S_2 via the polar coordinates $(\theta, \phi) \in [0, \pi] \times [0, 2\pi)$ and

$$g_m(\Omega) = \sqrt{\binom{2J}{m+J}} \times \left(\cos \frac{\theta}{2}\right)^{J+m} \left(\sin \frac{\theta}{2}\right)^{J-m} e^{i(J-m)\phi}. \quad (18)$$

The overlap between $\mathfrak{su}(2)$ CSs is

$$\langle \Omega | \Omega' \rangle = \left[\cos \frac{\theta}{2} \cos \frac{\theta'}{2} + \sin \frac{\theta}{2} \sin \frac{\theta'}{2} e^{-i(\phi - \phi')} \right]^{2J} \quad (19)$$

and

$$d\mu(\Omega) = \frac{2J+1}{4\pi} \sin \theta d\theta d\phi = \frac{2J+1}{4\pi} dm(\Omega), \quad (20)$$

with $dm(\Omega) := \sin \theta d\theta d\phi$ the measure on S_2 . The metric-induced distance between any two points on the sphere is

$$d(\Omega', \Omega'') = \arccos[\cos(\phi' - \phi'') \cos \theta' \cos \theta'' + \sin \theta' \sin \theta'']. \quad (21)$$

Before numerically simulating our gedanken experiment, we must estimate N_t , i.e., the value of N ensuring that the POVM described in Sec. IV satisfactorily discriminates the $\mathfrak{su}(2)$ CS of the system. This value depends neither on the state $|\Sigma\rangle$ nor on the specific tile to which it belongs; therefore, due to the rotational invariance of the metric and of the Husimi functions on S_2 , we can determine it by choosing $|\Sigma\rangle = |\Lambda_i\rangle$ and Λ_i as the north pole. With this choice, the first line of condition (15) is certainly fulfilled and from the second one we obtain that the following implication must hold:

$$\left(\cos \frac{\theta}{2}\right)^{2J} > \epsilon \Rightarrow \theta \leq \delta. \quad (22)$$

The value of N comes into play via the total momentum $J = \frac{1}{2}(N - n)$, with $0 \leq n \leq N$, so that condition (16) takes the

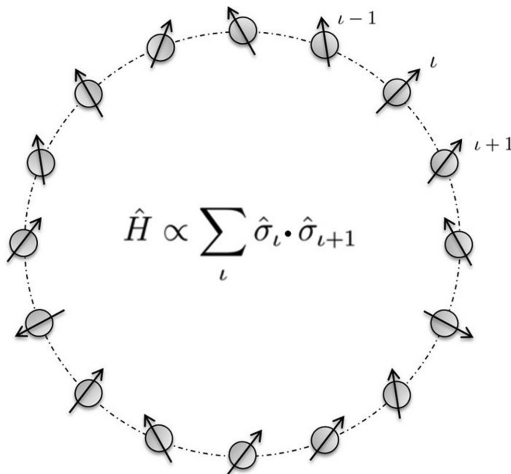


FIG. 3. Spin ring made of a finite number of $s = \frac{1}{2}$ distinguishable particles, each localized on one site of a circle. The operator shown in the center is an example of a Hamiltonian that commutes with the total spin of the ring.

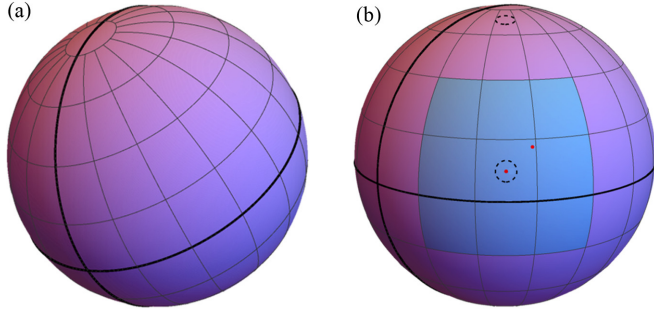


FIG. 4. The S_2 sphere with the tessellation used in this work. The points Λ_1 (the red dot centered in the tile) and Σ (the other red dot) are marked on the sphere in (b), where two circles of radius δ (dotted line) are also shown: The upper one defines δ itself via Eq. (14) and the lower one is that used in the example. The region in blue is the patch \tilde{I}_1 .

form

$$N > N_t = \frac{\ln \epsilon}{\ln[\cos(\delta/2)]} + n. \quad (23)$$

This is consistent with the fact that systems with a large magnetic moment ($N \gg 1$ and $n \ll N$) are well described by classical magnetism, while big systems ($N \gg 1$) with small magnetic moment ($n \leq N$) retain their quantum properties, regardless of their macroscopicity. The dependence of N_t on ϵ and δ underlines that even if the system has a very large J and seems to behave classically when observed with a slightly unfocused pair of goggles, small enough values of δ and ϵ always exist such that quantum-state indistinguishability cannot be circumvented and a classical-like description is flimsy. It is worth mentioning that the functional dependence of N_t in Eq. (23) and particularly the appearance of $\cos(\delta/2)$ follow from the expression of the overlap between $\text{su}(2)$ CSs [Eq. (19)], i.e., from the algebra $\text{su}(2)$ we are considering. Further comments on this point are made at the end of this section, where results obtained for different algebras are briefly reviewed.

We are now ready to describe the experiment. First we choose $\epsilon = 0.22$ ($\epsilon^2 \sim 0.05$). Then we consider a tessellation of S_2 into $L = 146$ tiles, made of two polar caps of radius $\frac{\pi}{18}$ and 144 tiles defined by 9 parallels at latitude $\theta_\ell = \frac{\pi}{2} + \ell \frac{\pi}{9}$, $\ell = -4, \dots, 4$, and 18 meridians at longitude $\phi_m = m \frac{\pi}{9}$, $m = 0, \dots, 17$ [see Fig. 4(a)]. According to (14), the parameter δ is the radius of the largest circle fully contained into the smallest tiles, i.e., those adjacent to the polar caps in our case, so $\delta = \arcsin(\sin \frac{\pi}{18} \sin \frac{\pi}{9}) \simeq 0.06$ [see Fig. 4(b)]. Therefore, from Eq. (23) with $n = 0$, we get $N_t = 3430$. As for the sampled GCS, we notice that each tile can be identified by a single index i biunivocally related to the couple (ℓ, m) , and the representative points Λ_i can be chosen as $\Lambda_i = ((4 + \ell) \frac{\pi}{9}, (m + \frac{1}{2}) \frac{\pi}{9})$. The tile I_1 is adjacent to the equator ($\ell = 0$) with $m = 2$, so $\Lambda_1 = (\frac{4}{9}\pi, \frac{5}{18}\pi)$ (the central red point on the sphere of Fig. 5). Refer to Appendixes B and C for more details and comments on the above choices.

Suppose the quantum system under investigation is in the unknown GCS $|\Sigma\rangle$ that we want to determine. In order to test our POVM we set $\Sigma = (0.88, 0.94)$ (the red point in the upper

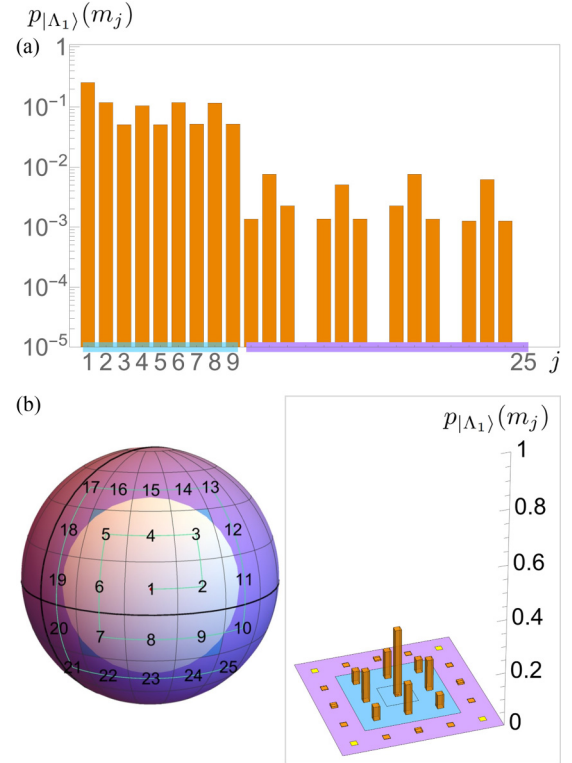


FIG. 5. The case $N = 30 \ll N_t$ with the system in the sampled GCS $|\Lambda_1\rangle$. (a) Probabilities (logarithmic scale) that the POVM outputs the result m_j associated with the j th tile via the scheme shown on the sphere in (b) on the left; indices labeling tiles that belong to the patch \tilde{I}_1 , $j = 1, 2, \dots, 9$, are marked in blue, as the patch itself. The region $S_{|\Lambda_1\rangle}$ is shown as a white area on the sphere. (b) On the right are the same data shown as columns (linear scale) on the plane tangent to the sphere in Λ_1 . Columns whose height is null are marked as yellow squares.

right corner of tile 1 on the spheres of Fig. 6) and see whether the POVM results allow us to identify the patch \tilde{I}_1 to which it belongs. To this aim we first consider the sampled GCSs and check the condition (12) taking 25 different results m_j , $j = 1, 2, \dots, 25$, each associated with the j th tile as shown in the spheres of Figs. 5–8, and evaluating the probability of obtaining each result if Γ is in the state $|\Lambda_1\rangle$, i.e.,

$$p_{|\Lambda_1\rangle}(m_j) = \int_{I_j^\delta \cap S_{|\Lambda_1\rangle}^\epsilon} d\mu(\Omega) |\langle \Lambda_1 | \Omega \rangle|^2, \quad (24)$$

according to Eq. (9) with $|\langle \Lambda_1 | \Omega \rangle|^2 < \epsilon^2 = 0.05$ set equal to 0, and $\langle \Lambda_1 | \Omega \rangle$ from Eq. (19) (for more details see Appendix C). The obtained probability distributions, illustrated in Figs. 5, 7, and 8 for $N = 30, 300$, and $3430 = N_t$, show that the result is certainly m_1 if $N = N_t$, while it can be different otherwise, meaning that $N \geq N_t$ is indeed a sufficient condition for the POVM to discriminate the sampled GCSs. The same analysis is done for the system in the (unknown, in principle) GCS $|\Sigma\rangle$, using the probability

$$p_{|\Sigma\rangle}(m_j) = \int_{I_j^\delta \cap S_{|\Sigma\rangle}^\epsilon} d\mu(\Omega) |\langle \Sigma | \Omega \rangle|^2. \quad (25)$$

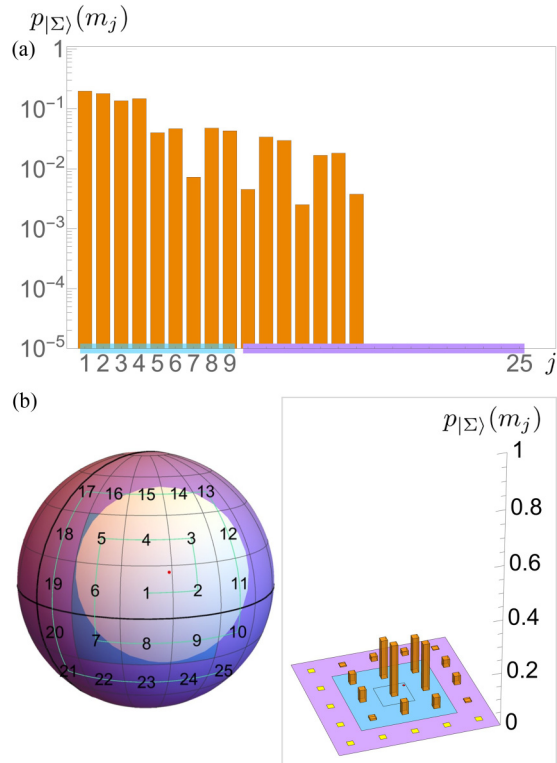


FIG. 6. The case $N = 30 \ll N_t$ with the system in the GCS $|\Sigma\rangle$. Details are the same as in Fig. 5 apart from the white area on the sphere that rather shows $S_{|\Sigma\rangle}^c$.

The probability distributions are shown in Figs. 6–8 for the same values of N as before. In this case the condition (13) is fulfilled not only for $N = N_t$ but also for $N = 300 < N_t$, as belonging to the patch \tilde{I}_1 is a much looser condition than that

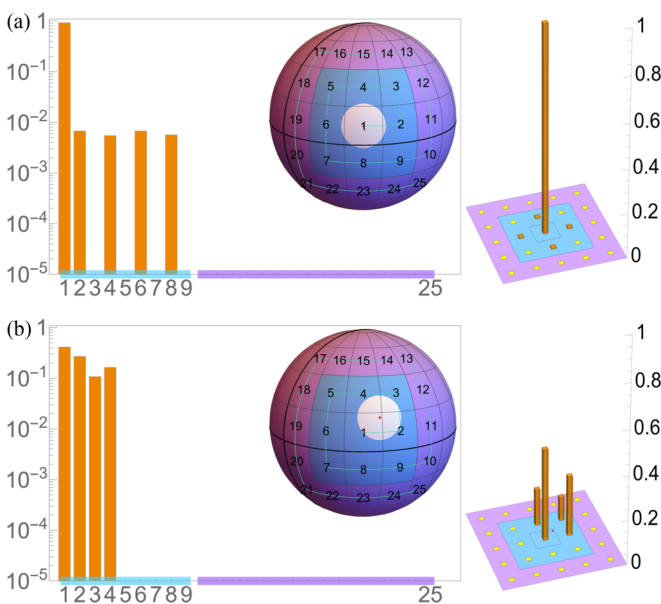


FIG. 7. The case $N = 300 < N_t$ with the system in (a) the sampled GCS and (b) the GCS $|\Sigma\rangle$. Details are the same as in Figs. 5 and 6.

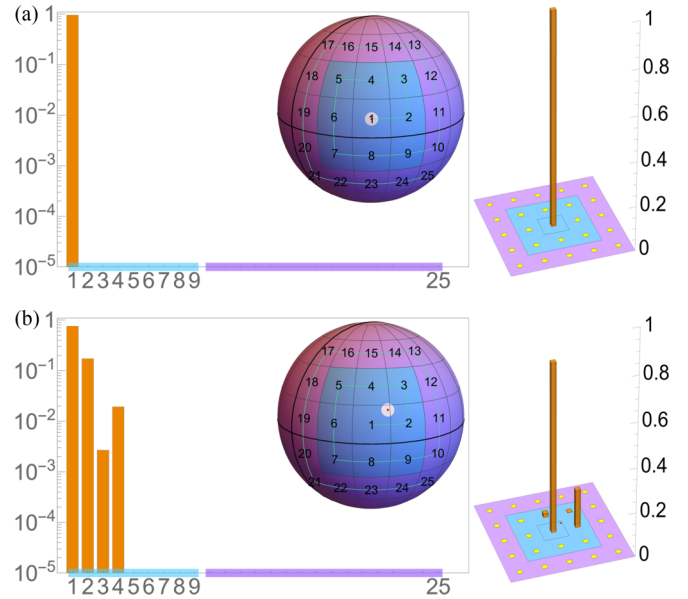


FIG. 8. The case $N = 3430 = N_t$ with the system in (a) the sampled GCS $|\Lambda_1\rangle$ and (b) the GCS $|\Sigma\rangle$. Details are the same as in Figs. 5 and 6.

belonging to the specific tile I_1 . However, if we cannot associate with absolute certainty the result m_1 with the sampled GCS Λ_1 , there is no reason why that same result should not correspond to a GCS with a representative point in the patch \tilde{I}_2 or in any other patch that contains I_1 . In this respect, we also underline that even if the probability distributions can tell to which specific tile the representative point Σ belongs, as seen in some of the above figures, in order for the emerging description to be of genuinely classical nature, this information must be available after the result of one single experiment, leaving aside the repetitions needed to deal with whatever experimental error. This is why the condition (12) must hold.

To summarize, the above example confirms that for $N > N_t$ the POVM results provide us with enough information to relate the state $|\Sigma\rangle$ of the system to the sampled representative point Λ_1 , with a systematic error controlled by the parameter δ that might bring such a point into Λ_j with $j = 2, 3, \dots, 9$. Evidently, a larger N can only improve the situation, while the experiment deteriorates as N is lowered.

VI. OTHER ALGEBRAS AND GENERAL COMMENTS

The example presented in Sec. V can serve as a template for systems described by different algebras, for which Eqs. (19) and (21) must be replaced with the expressions proper to the specific algebra and geometry of the respective manifolds. In particular, for pseudospin systems [$\mathfrak{su}(1, 1)$ algebra and manifold pseudosphere PS_2] we obtain

$$N_t = \frac{-\ln \epsilon}{2k \ln[\cosh(\delta/2)]}, \quad (26)$$

with k the Bargmann index of the single pseudospin, and for bosonic systems (\mathfrak{h}_4 and manifold complex plane)

$$N_t = -\frac{1}{\delta^2} \ln \epsilon, \quad (27)$$

where different relations between the parameter N and the relevant coefficients of the algebra hold, analogous to $N = 2(J - n)$ in the magnetic case presented above [3]. Note that the functional dependence of N_t on ϵ is always the same (direct proportionality to $\ln \epsilon$), while different algebras introduce different dependences on δ . This reflects the different nature and meaning of the two parameters, as further discussed below.

Equations (23), (26), and (27) can be used in a different way, i.e., keeping N fixed to obtain the features of the best attainable classical-like description, for that value of N . This is understood by noting that the size of the regions $S_{|\Sigma}^\epsilon$ are gauged by N via the condition (5), as explicitly shown in the above example and figures. In more detail, looking, for instance, at Eq. (27), one understands that for a given N the possible classical-like description will have a limited resolution (δ^2 cannot be smaller than $-N^{-1} \ln \epsilon$) and a certain degree of unavoidable indeterminacy [ϵ must be larger than $\exp(-N\delta^2)$]. It is not by chance that the same type of limitation on the accuracy of the picture provided by an experimental observation is expressed by uncertainty relations. In fact, the lower bound of any Robertson-Schrödinger uncertainty relation, whose finiteness embodies the uncertainty and whose value quantifies its extent, is proportional to the expectation value of some Lie bracket representation. These brackets are monotonically decreasing functions of N , which vanish for $N \rightarrow \infty$, for all known quantum theories (they are proportional to $1/N$ in the theories here considered). Via this dependence, the uncertainty relations set natural bounds on δ and ϵ , fundamentally limiting the resolution of the apparatus and the deterministic nature of the classical-like description that one can obtain, respectively.

The interplay between the three parameters N , ϵ , and δ can also be seen from a different viewpoint, gained by considering N fixed and not necessarily large. In fact, from Eqs. (23), (26), and (27) it follows that in order for a small N to be larger than N_t , as needed to obtain a classical-like description of some sort, we must either choose $\epsilon \simeq 1$ or design an experimental apparatus with $\delta \gg 1$. The first case corresponds to accepting such a low sensitivity that only a paltry number of outputs is made available, no matter how many times we repeat the experiment, leading to an essentially inefficient procedure [referring to Eq. (C3), this means $p_{|\Sigma}(\text{null}) \sim 1$]. In the second case $\delta \gg 1$, the tiles are so big that only a few GCSs are sampled, leading to an unsatisfactory resolution of the apparatus and an unfaithful classical-like description. As expected, then “small” quantum systems cannot be described in terms of a classical formalism, regardless of their being in some GCSs or not. This does not mean that procedures for quantum state discrimination cannot be designed for small N . In fact, procedures of such a type have been designed and demonstrated to be highly efficient also for GCSs [24], but they clearly do not make a classical-like description of the observed system.

Before moving to some closing remarks, let us briefly comment on the possibility of using the proposed strategy to classically describe not only the state of a system, but also its dynamical evolution, a possibility following from the fact that GCSs evolve into other GCSs by definition, as mentioned in Sec. II. In our setting, this feature implies the following.

Consider a system with $N > N_t(\epsilon, \delta)$ for some given ϵ and δ and assume that, at some time t_0 , it is in the GCS $|\Sigma\rangle$ with $\Sigma \in I_i^\delta$. Let $\gamma(t) : \gamma(t_0) = \Sigma$ be the trajectory drawn by its representative point on \mathcal{M} . Then if $\gamma(t) \in I_i^\delta \forall t$ there is no observable dynamics at the classical level and if there exists $t_1 > t_0$ such that $\gamma(t) \notin I_i^\delta$ for $t > t_1$ a dynamics emerges at the classical level in which the classical state is well described by $m_{i(0)}$ until t_1 , becomes better described by some other $m_{i(1)}$ until a later time t_2 , and so forth. The discreteness of the tessellation is responsible for a discontinuous representation of the GCS dynamics in terms of the time-ordered sequence of results $m_{i(0)}, m_{i(1)}, m_{i(2)}, \dots$; however, the jump from one result to the successive one is preceded by an increase and followed by a decrease of the systematic error (due to the fact that the representative point gets closer to the tiles borders) that smoothens the (otherwise stepped) experimentally obtained trajectory. As for the typical time during which the classical state corresponds to just one specific result m_i , we expect it is related to the size of the tiles, as gauged by δ , in a way that depends on the Hamiltonian couplings. This type of analysis goes beyond the scope of this work, but it can be certainly developed, both in general and in the specific case of the isotropic Heisenberg interaction considered in Sec. V.

VII. CONCLUSION

In this work we have seen that a physical system, quantum by nature, can possibly be described in “classical words” if the number N of elements that determines the global algebra defining its GCS is larger than a threshold value that depends on parameters of our choice. The classical words are the tools of the Hamiltonian formalism, with the state of the system described by a representative point on a specific phase space and the possibility of getting information upon the state of the system via one single measurement, a possibility that is precluded in quantum mechanics. In this respect, referring to the example of Sec. V, our choice of showing the probability distributions in Figs. 5–8 is functional to a description that is ultimately quantum. However, if one knows δ , chooses ϵ , determines $N_t(\epsilon, \delta)$, and checks that $N > N_t$, then the single result m_i identifies the classical representative point of the system Λ_i with the usual systematic experimental error due to the resolution of the measuring apparatus, here gauged by δ . The entity of the probability that the actual representative point be different from Λ_i can be set arbitrarily small by reducing ϵ : This probability is the residual quantum signature that one can decide to ignore, as done with the probability that a human being passes through a wooden door. As for the precise definition and value of δ , they depend on the experimental apparatus and can be difficult to obtain. Obviously, one can always choose a value for δ which is larger than the one that ideally translates the conditions (12) and (13) into the implication (15); however, this may lead to an unnecessary overestimation of N_t . A thorough discussion of these aspects can be found in Appendix B.

The two small numbers δ and ϵ have an essential role in our picture: They are quantifiers of the available experimental resolution and of our willingness to neglect rare events, respectively, and should not be considered as expansion parameters ruling the validity of some semiclassical

approximation. In fact, our proposal is alternative to semi-classical approximations and can also be used in a somehow opposite direction, namely, to study if and how a system originally described by a classical theory can manifest more and more marked quantum traits as its size reduces for one reason or another. In this regard, work is in progress to use this approach to study how a Schwarzschild black hole, i.e., an object which is classically described by definition, can manifest increasingly evident quantum features as its size shrinks due to the emission of Hawking radiation [25]. We believe that a better understanding of this crossover can shed light upon the information paradox and its relation with the Page curve [26,27], as well as on the way spacetime can arise in the fully algebraic setting of standard quantum mechanics [28].

ACKNOWLEDGMENTS

N.P. gratefully acknowledges the Magnus Ehrnrooth Foundation for financial support. The work of P.V. was in the framework of the Convezione Operativa between the Institute for Complex Systems of CNR and the Department of Physics and Astronomy of the Università degli Studi di Firenze.

APPENDIX A: MONGE DISTANCE

In this Appendix we provide details on the Monge distance between probability distributions and its generalization to quantum states. The Monge distance was introduced to model the most efficient strategy of transporting a pile of soil from one place to another [15]. Specifically, one can describe the position and shape of the initial and final soil configurations via the probability distributions q_1 and q_2 , respectively. Let us assume these are defined in an open set \mathbb{O} of a metric space (\mathbb{M}, d) endowed with a normalized measure $d\mu$. Given that $q_i \geq 0$ and $\int_{\mathbb{O}} q_i d\mu = 1$, one can recover the intuition behind the transport problem by defining

$$V_i = \{(x, y) \in \mathbb{O} \times \mathbb{R}^+ : 0 \leq y \leq q_i(x)\} \quad (A1)$$

as the volume of the mound associated with q_i . Then any transport strategy for moving q_1 to q_2 is related to a continuous one-to-one function T , mapping \mathbb{O} to itself and called a plan. Moreover, it is required that these plans are volume preserving, i.e.,

$$\int_{\mathbb{A}} q_1 d\mu = \int_{T^{-1}(\mathbb{A})} q_2 d\mu \quad \forall \mathbb{A} \subset \mathbb{M}. \quad (A2)$$

The Monge distance between probability distributions is defined as

$$d_M(q_1, q_2) = \inf_T \left\{ \int_{\mathbb{O}} d(x, T(x)) q_1(x) d\mu(x) \right\}, \quad (A3)$$

where the minimization is performed over the set of all plans. When it exists, the optimal plan that realizes the minimum in Eq. (A3) is called a Monge plan. For the pathological situations in which a Monge plan does not exist, Kantorovich introduced a weakened version of the Monge distance [16], called the Monge-Kantorovich distance; however, the Monge distance discussed here is sufficient for our purposes.

When considering probability distributions defined on the real line equipped with the Euclidean distance, Eq. (A3) becomes

$$d_M(q_1, q_2) = \int_{-\infty}^{\infty} |Q_1(x) - Q_2(x)| dx, \quad (A4)$$

where Q_i are the cumulative distributions of q_i [29]. Despite being specific to the one-dimensional case, when supplemented with symmetry arguments the above expression can be used to find the Monge distance for some two-dimensional problems. In general, though, finding an analytical expression for $d_M(q_1, q_2)$ without relying on numerical algorithms is most often an impossible task; a vast amount of literature on computational approaches to the transport problem is available (see, for instance, Ref. [30]). The Monge distance can be used to define a distance between quantum states [17,22,31]. Referring to the group-theoretic construction of GCSs presented in Sec. II and recalling that the Husimi functions (3) are probability distributions on the GCS manifold \mathcal{M} , a distance between quantum states can be defined via

$$d_M(|\phi\rangle, |\psi\rangle) \equiv d_M(H_\phi, H_\psi), \quad (A5)$$

where $|\phi\rangle, |\psi\rangle \in \mathcal{H}$ and the distance on the right-hand side is obtained via Eq. (A3) by selecting \mathcal{M} and the metric-induced distance for the metric space (\mathbb{M}, d) . Other definitions of quantum distances via the transport problem have been proposed recently [32,33], but d_M has some particularly useful properties. First, the inequality (6) holds (with the equality certainly obtained as $N \rightarrow \infty$), which provides a convenient upper bound to the Monge distance, whenever it is hard to be evaluated. Second, from the translation invariance of the measure and metric-induced distance on \mathcal{M} it follows that the Monge distance between quantum states is invariant under the action of the elements of the group G that defines the quantum theory.

The closed form of the Monge distance between any two $su(2)$ CSs is obtained in Ref. [22]. Referring to the discussion in Sec. V, due to the rotational invariance of the problem, the Monge distance between any two $su(2)$ CSs only depends on the azimuthal coordinate, the angle θ , of the point corresponding to one of them, in a polar reference system where the point corresponding to the other is the north pole:

$$d_M(J; \theta) = \pi \sin\left(\frac{\theta}{2}\right) W_J \left[\sin^2\left(\frac{\theta}{2}\right) \right]. \quad (A6)$$

Here

$$W_J(x) = \frac{2J+1}{4^{J+1}} \sum_{0 \leq u, v, u+v=J} S_J(u, v) A(u, v) x^u (1-x)^v, \quad (A7)$$

with

$$S_J(u, v) = \frac{(2J)!}{[2J - 2(u+v) - 1]! u! v! (u+v+1)! 4^{u+v}} \quad (A8)$$

and

$$A(u, v) = \sum_{s=v+1}^{\infty} \frac{\binom{2s}{s}}{(u+s+1)4^s}. \quad (A9)$$

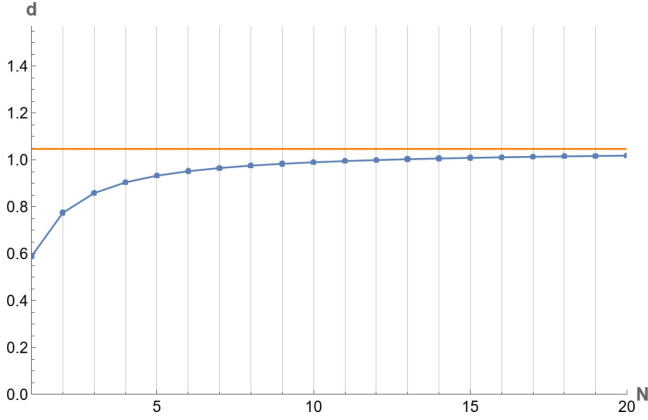


FIG. 9. Monge distance (blue dots) and metric-induced distance (orange line) between the $\text{su}(2)$ CS related to the points $(0,0)$ and $(\pi/3, 0)$, as functions of J . As expected, for increasing J the Monge distance approaches the metric-induced one from below.

The large- N limit of Eq. (A6) is

$$\lim_{J \rightarrow \infty} d_M(J; \theta) = \theta. \quad (\text{A10})$$

In Fig. 9 we show $d_M(J; \pi/3)$, as numerically obtained after Eq. (A6) for $J \in [1, 20]$, and compare it with the metric-induced distance, which does not depend on J .

APPENDIX B: δ AND TESSELLATION OF S_2

The S_2 tessellation used for S_2 in Sec. V is the case $k = 4$ of a tessellation $T(k)$ defined by $2k + 1$ parallels and $2(2k + 1)$ meridians, according to

$$\begin{aligned} \theta_l &= \frac{\pi}{2} + l \frac{\pi}{2k+1}, \quad l = -k, \dots, k \quad (\text{parallels}), \\ \phi_m &= m \frac{\pi}{2k+1}, \quad m = 0, \dots, 2(2k+1) \quad (\text{meridians}), \end{aligned} \quad (\text{B1})$$

where the meridians are considered only for $\theta \in [\theta_{-k}, \theta_k]$. The number of tiles is $L = 2(4k^2 + 2k + 1)$, including the two polar caps of radius $\pi/(4k + 2)$. In each tile, the point $\Lambda_i = (\theta_{\Lambda_i}, \phi_{\Lambda_i})$ corresponding to the sampled GCS $|\Lambda_i\rangle$ is the center of the largest circle inscribed in the tile itself. Overall, these are the two poles and the points with coordinates $(\frac{\pi}{2} + (2l - 1)\frac{\Delta}{2}, (2m + 1)\frac{\Delta}{2})$, with $\Delta = \pi/(2k + 1)$, $l = -k + 1, \dots, k$, and $m = 0, \dots, 2(2k + 1) - 1$. For a generic point $\Sigma = (\theta_\Sigma, \phi_\Sigma)$ on the tile identified by the pair (l, m) , one can write $\theta_\Sigma = \frac{\pi}{2} + (l - y)\Delta$, $\phi_\Sigma = (m + x)\Delta$, with $(y, x) \in [0, 1] \times [0, 1]$. The parameter δ , defined by Eq. (14) as the radius of the largest circle inscribed in the smallest tiles (those identified by $l = -k + 1$ or $l = k$), is

$$\delta = \arcsin \left[\sin \left(\frac{\Delta}{2} \right) \sin \Delta \right]. \quad (\text{B2})$$

The connection between the geometric conditions (12) and (13) and the algebraic inequality in (15), with δ defined in (14), follows from the specific setting one is considering. In fact, whether or not an exact match exists depends on the geometry of the problem, the tessellation chosen, and the definition of the parameter δ , which can be modified in order

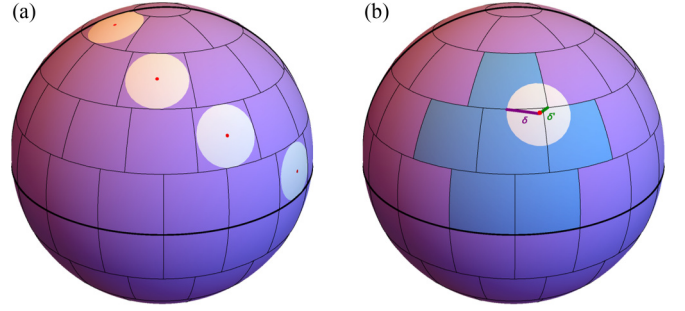


FIG. 10. Tessellation $T^{\textcircled{4}}$ with (a) the regions $S_{|\Lambda_i}^\epsilon$ (in white) with the points Λ (in red), corresponding to sampled GCSs, at various latitudes and (b) the region $S_{|\Sigma}^\epsilon$ (in white) with the point Σ (in red), representing a generic GCS, and the corresponding patch (in blue).

to better fit the specific problem and the related experimental apparatus. Consider, for instance, a tessellation $T^{\textcircled{4}}$, a sibling of $T(4)$, defined by parallels and shifted chunks of meridians such that the radius of the largest circle inscribed in each tile is $\pi/18$ and the points corresponding to the sampled GCS are the centers of such circles. Figure 10(a) shows $T^{\textcircled{4}}$ and the region $S_{|\Lambda_i}^\epsilon$ defined by Eq. (11) at various latitudes, for $\epsilon = 0.22$ and $N = 400 > N_t = 398$, from Eq. (23). As expected, since N is above threshold, the condition ensuring that sampled GCSs are distinguishable, i.e., the condition (12), is fulfilled, as seen in Fig. 10(a). On the other hand, there is no patch \tilde{I}_i that fully contains $S_{|\Sigma}^\epsilon$ for $|\Sigma\rangle$ with a representative point [the red dot in Fig. 10(b)]. For this specific GCS, in fact, the parameter δ , as defined by Eq. (14) and represented by the length of the purple line in Fig. 10(b), should be replaced by the length δ' of the green line. This done, Eq. (23) provides $N'_t = 3285 \gg N_t = 398$, confirming that we are indeed working below threshold. Notice that by changing the red point, for instance, moving it closer to the upper right corner of the corresponding tile, the value of N'_t can become even greater. In fact, to obtain a value of N_t that works for any point given the specific tessellation, one should replace Eqs. (14) and (15) with

$$\delta := \min_i \left[\min_{\Omega \in \partial I_i} d(\Omega, \Lambda_i), \min_{\Omega \in \partial I_i, \tilde{\Omega} \in \partial \tilde{I}_i} d(\Omega, \tilde{\Omega}) \right] \quad (\text{B3})$$

and

$$|\langle \Omega | \Sigma \rangle| > \epsilon \Rightarrow d_M(|\Omega\rangle, |\Sigma\rangle) \leq \delta \forall \Omega, \Sigma \in S_2. \quad (\text{B4})$$

APPENDIX C: ϵ AND PROBABILITY HISTOGRAMS

In our approach it is necessary to consider null any inner product whose modulus is less than a chosen (small) positive value ϵ ,

$$|\langle \Sigma | \Omega \rangle| \leq \epsilon \Leftrightarrow |\langle \Sigma | \Omega \rangle| \simeq 0 \forall \Sigma, \Omega \in \mathcal{M}. \quad (\text{C1})$$

As a consequence, the probability (9) is replaced by

$$p_{|\Sigma\rangle}(m_i) = \int_{I_i^{\textcircled{4}} \cap S_{|\Sigma}^\epsilon} d\mu(\Omega) |\langle \Sigma | \Omega \rangle|^2, \quad (\text{C2})$$

meaning that there is a finite probability that the experimental apparatus does not produce a meaningful output (due to the

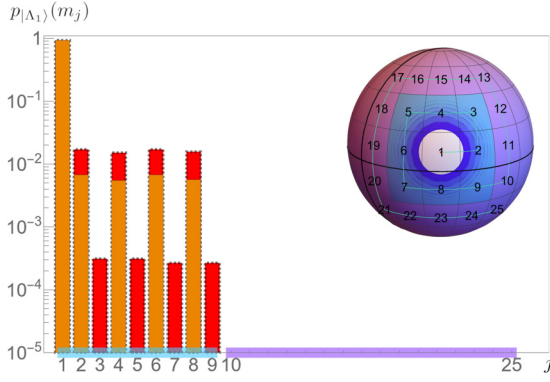


FIG. 11. The case $N = 300 < N_t$ with the system in the sampled GCS $|\Lambda_1\rangle$. Probabilities (logarithmic scale) that the POVM outputs the result m_j associated with the j th tile via the scheme shown on the sphere and other details as in Figs. 5–8; bars with dashed black edges are the exact probabilities from Eq. (9), orange bars are approximated probabilities from Eq. (24) with $\epsilon = 0.22$, and the difference is in red. The contour plot of the Husimi function centered in Λ_1 (blue shades) and the region $S_{|\Lambda_1\rangle}^\epsilon$ (white circle) are also shown on the sphere.

reliability of the proposed description) which is, when the system is in the state $|\Sigma\rangle$,

$$p_{|\Sigma\rangle}(\text{null}) = \int_{\mathcal{M} \setminus S_{|\Sigma\rangle}^\epsilon} d\mu(\Omega) |\langle \Sigma | \Omega \rangle|^2. \quad (\text{C3})$$

In the specific case considered in Sec. V, the spherical symmetry implies that $p_{|\Sigma\rangle}(\text{null})$ does not depend on $|\Sigma\rangle$. Therefore, one can choose Σ as the north pole in Eq. (C3) and get the total probability that the experimental apparatus provides no output, irrespective of the state of the system,

$$p(\text{null}) = \frac{2J+1}{4\pi} \int_0^{2\pi} d\phi \int_{\arccos(\epsilon^{1/2J})}^\pi d\theta \left(\cos \frac{\theta}{2}\right)^{4J} \sin \theta = \epsilon^{2+1/J}. \quad (\text{C4})$$

For the tessellation $T(4)$ with $\epsilon = 0.22$ and $N = N_t = 3430$, it is $p(\text{null}) \sim 0.0483$. Consequently, the probabilities shown in Figs. 5–8 do not sum to one (we have opted for this solution for the sake of a clearer discussion). For comparison, in Figs. 11 and 12 we show the exact probabilities from

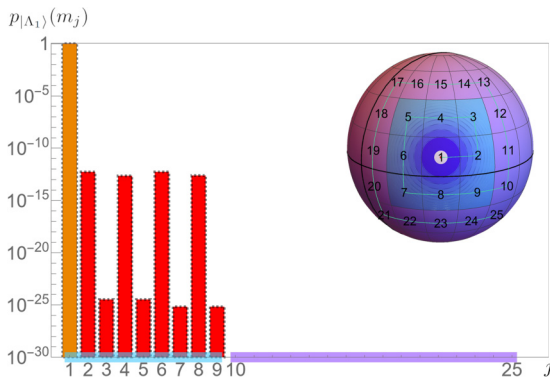


FIG. 12. The case $N = 3430 = N_t$. The details are the same as in Fig. 11.

Eq. (9) (bars with black dashed borders), the approximated probabilities from Eq. (24) (in orange), and their difference (in red), for $N = 300 < N_t$ and $N = 3430 = N_t$, respectively, with the system in the sampled GCS Λ_1 , as in Figs. 6(a) and 7(a). Notice that, since $N < N_t$ in Fig. 11, some of the bars with dashed borders relative to the results $m_{j \neq 1}$ are not completely colored red. On the other hand, consistently with the fact that $N \geq N_t$ and that $|\Lambda_1\rangle$ is a sampled GCS, all the bars with dashed borders of Fig. 12 relative to the results $m_{j \neq 1}$ are red.

APPENDIX D: GCS SUPERPOSITION

The restriction of our work to quantum systems in GCSs follows from the question from which we started, namely, when is a system amenable to a classical-like description? In fact, if the system is in a GCS of the quantum theory that describes it, this question can have a positive answer, as originally demonstrated by Yaffe [2], Lieb [19], and Berezin [20] and others. The necessity of this condition has not been formally demonstrated yet (see Sec. VII of Ref. [2] for a thorough discussion on this point), but no counterexample has been found either. One of the simplest and most convincing way to see why only GCSs can survive the quantum-to-classical crossover is to consider that a symplectic manifold must emerge in such a crossover (to become the classical phase space), with each of its points corresponding both to a quantum and to a classical state and the quantum unitary dynamics defining trajectories on that same manifold. While this is naturally provided by the GCS construction, no other formalism seems to succeed in such a task. A discussion about if and why quantum states must be coherent if they were to flow into well-defined classical states is of great interest to us, but is not the purpose of this work. However, in this Appendix we investigate what happens if the system is not assumed in a GCS, but rather in a superposition of two different GCSs, which is not a GCS, as easily seen from the definition (1). Consider the state

$$|\psi\rangle = \alpha |\Sigma\rangle + \beta |\Sigma'\rangle. \quad (\text{D1})$$

If $N > N_t$ and $\Sigma \in I_i^\delta$ three cases can occur: (i) Σ and Σ' are in the same tile I_i^δ , (ii) Σ' is in the patch \tilde{I}_i^δ such that $\Sigma \in I_i^\delta$, and (iii) Σ' is outside the patch \tilde{I}_i^δ such that $\Sigma \in I_i^\delta$. In the first case, an observer performing the POVM described in Sec. IV would obtain outcomes essentially identical to those obtained when the system is in any other GCS in I_i^δ . On the contrary, in the second and third cases the observer cannot unequivocally associate the outcomes with one single sampled GCS and the classical description is hence unattainable. In other terms, a classical-like description is viable for systems that are superpositions of GCSs if and only if the respective representative points on \mathcal{M} are all contained in the same tile, say, I_i^δ ; an observer would see such system in the classical state with representative point Λ_i ,

$$p_{|\Sigma\rangle}(m_j). \quad (\text{D2})$$

- [1] S. W. Hawking, Particle creation by black holes, *Commun. Math. Phys.* **43**, 199 (1975).
- [2] L.G. Yaffe, Large N limits as classical mechanics, *Rev. Mod. Phys.* **54**, 407 (1982).
- [3] A. Coppo, A. Cuccoli, C. Foti, and P. Verrucchi, From a quantum theory to a classical one, *Soft Comput.* **24**, 10315 (2020).
- [4] J. Kofler and C. Brukner, Classical World Arising out of Quantum Physics under the Restriction of Coarse-Grained Measurements, *Phys. Rev. Lett.* **99**, 180403 (2007).
- [5] M. H. Muñoz-Arias, I. H. Deutsch, P. S. Jessen, and P. M. Poggi, Simulation of the complex dynamics of mean-field p -spin models using measurement-based quantum feedback control, *Phys. Rev. A* **102**, 022610 (2020).
- [6] P. Busch, J. P. Lathi, and P. Mittelstaedt, *The Quantum Theory of Measurement* (Springer, Berlin, 1996).
- [7] M. A. Nielsen and I. L. Chuang, *Quantum Computation and Quantum Information* (Cambridge University Press, Cambridge, 2016).
- [8] T. Heinosaari and M. Ziman, *The Mathematical Language of Quantum Theory* (Cambridge University Press, Cambridge, 2012).
- [9] W. M. Zhang, D. H. Feng, and R. Gilmore, Coherent states: theory and some applications, *Rev. Mod. Phys.* **62**, 867 (1990).
- [10] A. M. Perelomov, *Generalized Coherent States and Their Applications* (Springer, Berlin, 1986).
- [11] M. Combes and D. Robert, *Coherent States and Applications in Mathematical Physics* (Springer, Dordrecht, 2012).
- [12] J. M. Lee, *Introduction to Smooth Manifolds* (Springer, Berlin, 2003).
- [13] K. Husimi, Some formal properties of the density matrix, *J. Phys. Soc. Jpn.* **22**, 264 (1940).
- [14] C. Zachos, D. Fairlie, and T. Curtright, *Quantum Mechanics in Phase Space: An Overview with Selected Papers* (World Scientific, Singapore, 2005).
- [15] G. Monge, *Mémoire sur la Théorie des Déblais et des Remblais* (De l'Imprimerie Royale, Paris, 1781), pp. 666–704.
- [16] L. V. Kantorovich, On a problem of Monge, *J. Math. Sci.* **133**, 1383 (2006).
- [17] K. Zyczkowski and W. Slomczynski, The Monge distance between quantum states, *J. Phys. A: Math. Gen.* **31**, 9095 (1998).
- [18] M. Thorpe, Introduction to optimal transport, lecture notes, University of Cambridge, 2018.
- [19] E. H. Lieb, The classical limit of quantum spin systems, *Commun. Math. Phys.* **31**, 327 (1973).
- [20] F. A. Berezin, Models of Gross-Neveu type are quantization of a classical mechanics with nonlinear phase space, *Commun. Math. Phys.* **63**, 131 (1978).
- [21] C. Foti, T. Heinosaari, S. Maniscalco, and P. Verrucchi, Whenever a quantum environment emerges as a classical system, it behaves like a measuring apparatus, *Quantum* **3**, 179 (2019).
- [22] K. Zyczkowski and W. Slomczynski, The Monge metric on the sphere and geometry of quantum states, *J. Phys. A: Math. Gen.* **34**, 6689 (2001).
- [23] S. M. Barnett and S. Croke, Quantum state discrimination, *Adv. Opt. Photon.* **1**, 238 (2009).
- [24] A. R. Ferdinand, M. T. DiMario, and F. E. Becerra, Multi-state discrimination below the quantum noise limit at the single-photon level, *npj Quantum Inf.* **3**, 43 (2017).
- [25] N. Pranzini, The strange case of a black hole, which is classical, and yet has quantum traits, M.Sc. thesis, University of Florence, 2020.
- [26] D. N. Page, Information in Black Hole Radiation, *Phys. Rev. Lett.* **71**, 3743 (1993).
- [27] A. Almheiri, R. Mahajan, J. Maldacena, and Y. Zhao, The Page curve of Hawking radiation from semiclassical geometry, *J. High Energy Phys.* **3** (2020) 149.
- [28] C. Foti, A. Coppo, G. Barni, A. Cuccoli, and P. Verrucchi, Time and classical equations of motion from quantum entanglement via the Page and Wootters mechanism with generalized coherent states, *Nat. Commun.* **12**, 1787 (2021).
- [29] T. Salvemini, *Atti della VI Riunione della Società Italiana di Statistica, Roma, 1943* (CISU, Rome, 1943).
- [30] A. M. Oberman and Y. Ruan, An efficient linear programming method for optimal transportation, [arXiv:1509.03668](https://arxiv.org/abs/1509.03668).
- [31] I. Bengtsson and K. Zyczkowski, *Geometry of Quantum States: An Introduction to Quantum Entanglement* (Cambridge University Press, Cambridge, 2006).
- [32] S. Friedland, M. Eckstein, S. Cole, and K. Zyczkowski, Quantum Monge-Kantorovich Problem and Transport Distance between Density Matrices, *Phys. Rev. Lett.* **129**, 110402 (2022).
- [33] S. Cole, M. Eckstein, S. Friedland, and K. Zyczkowski, Quantum optimal transport, [arXiv:2105.06922](https://arxiv.org/abs/2105.06922).